Cellulose nanocrystals as templates for cetyltrimethylammonium bromide mediated synthesis of Ag nanoparticles and their novel use in PLA films

E. Evrim Yalcinkaya[1], D. Puglia[2*], E. Fortunati[2], F. Bertoglio[3,4], G. Bruni[4], L. Visai[3,6], J.M. Kenny[2]

[1]*Ege University Faculty of Science Chemistry Department, 35100, Bornova-Izmir/Turkey*
[2]*University of Perugia, Civil and Environmental Engineering Department, UdR INSTM, Strada di Pentima 4, Italy*
[3]*Molecular Medicine Department (DMM), Center for Health Technologies (CHT),UdR INSTM, University of Pavia, Via Taramelli 3/B, 27100 Pavia, Italy*
[4]*Scuola Universitaria Superiore IUSS, 27100 Pavia, Italy*
[5]*Department of Chemistry, — Physical-Chemistry Section, University of Pavia, Viale Taramelli 16, 27100, Pavia, Italy*
[6]*Department of Occupational Medicine, Toxicology and Environmental Risks, Istituti Clinici Scientifici Maugeri S.p.A., IRCCS, Via S. Boezio, 28, 27100, Pavia, Italy*

Abstract

In the present paper, we report how cellulose nanocrystals (CNC) from microcrystalline cellulose have the capacity to assist in the synthesis of metallic nanoparticle chains. A cationic surfactant, cetyltrimethylammonium bromide (CTAB), was used as modifier for CNC surface. Silver nanoparticles were synthesized on CNC, and the nanoparticle density and size were optimized by varying the concentration of the nitrate and reducing agent, and the reduction time. The experimental conditions were optimized for the synthesis and the resulting Ag grafted CNC (Ag-g-CNC) were characterized by means of TGA, SEM and SAXS, and then introduced in PLA matrix. PLA nanocomposite containing silver grafted cellulose nanocrystals (PLA/0.5Ag-g-1CNC) was characterized by optical and thermal analyses and the obtained data were compared with results from PLA nanocomposites containing 1% wt of CNC (PLA/1CNC), 0.5% wt of silver nanoparticles (PLA/0.5Ag) and hybrid system containing CNC and silver in the same amount (PLA/1CNC/0.5Ag). The results demonstrated that grafting of silver nanoparticles on CNC positively affected the thermal degradation process and cold crystallization processes of PLA matrix. Finally, the antibacterial activity of the different systems was studied at various incubation times and temperatures, showing the best performance for PLA/1CNC/0.5Ag based nanocomposite.

Keywords: cellulose nanocrystals, silver nanoparticles, grafting, chemical modification, poly (lactic acid), nanocomposites, antibacterial.

*Corresponding author. Tel.: +39-0744492916; fax: +39-0744492950;
E-mail address: debora.puglia@unipg.it

1. Introduction

In the last decades, there has been great progress in the colloidal synthesis of inorganic nanoparticles that have received great attention, due to their unique optical, electronic, magnetic, antimicrobial properties. Their small size, large specific surface area and tuneable physical-chemical properties that differ significantly from the bulk analogues led to intense research on their use in composite materials (Thomas et al., 2008). A key aspect to consider, when combining metal nanoparticles with cellulose fibres, is the methodology to be employed, namely by taking in consideration the envisaged applications. A number of approaches have been developed to attach metal nanoparticles onto cellulose fibres: the preparation of cellulose/metal nanocomposites by the in-situ reduction of metal salts in cellulose aqueous suspensions has been extensively investigated for the production of silver (Pinto et al., 2009; Yang et al., 2012). Another commonly used in-situ approach to prepare metal dispersion in cellulose matrices involves the entrapment of metal cations in the fibres followed by their reduction with an external reducing agent (such as sodium borohydride). Some reports have described the loading of silver nanoparticles into grafted filter paper (Tankhiwale & Bajpai, 2009) and bacterial cellulose (Marques et al., 2008). In addition, natural biopolymers in the form of cellulose nanocrystals (CNC), due to their unique and well-defined physical-chemical properties, are shown to have the required characteristics to serve as chemically reactive biotemplates for metallic and semiconductor nanomaterial synthesis. Silver nanoparticle chains may be synthesized on CNC by exposing metallic precursor salts to a cationic surfactant, cetyltrimethylammonium bromide (CTAB), and a reducing agent. The nanoparticle

density and particle size may be controlled by varying the concentration of CTAB, pH of the salt solution, as well as the reduction time or reaction time between the reducing agent and the metal precursor (Cai et al., 20009; J; Shin et al., 2008; Liu et al., 2011; Padalkar et al., 2010; Drogat et al., 2011). The proposed mechanism for the synthesis of Ag nanoparticles on the CNC surfaces considers that Ag nanoparticles are formed via the conventional reduction of $AgNO_3$, CTAB (cetyltrimethylammonium bromide) acting as a nanoparticle stabilizer. The cationic has been utilized not only as a stabilizer of metallic nanoparticles but also as a vehicle for the positioning of these particles on the CNC surface (Padalkar et al., 2010). The results shed light on the methods to stabilize metal nanoparticles, control their nucleation, and highlight the potential of CNC in metal nanoparticle synthesis (Zhou et al.,2013; Lokanathan et al.,2014). Considering the functional properties of CNC and metallic nanoparticles, their incorporation as bifunctional fillers in PLA is expected to improve mechanical and antimicrobial properties of the matrix. It is finally clear that an extensive and copious literature exists on the use of cellulose nanoreinforcements and metal nanoparticles as hybrid systems in PLA matrix (Fortunati et al., 2013a; Fortunati et al., 2014; Cacciotti et al., 2014) and PLA film containing silver impregnated cellulose (Vivekanandhan e t al., 2012) while, at the best of our knowledge, there are no examples in the literature of the use of silver grafted cellulose nanocrystals in solvent casted PLA films.

In the present work, the synthesis of silver nanoparticles on CNC extracted from microcrystalline cellulose (MCC) mediated by CTAB was studied and optimized, and the resulting Ag grafted CNC (Ag-g-CNC) were characterized by means of TGA, SEM and SAXS. The produced Ag-g-CNC were then introduced in PLA thermoplastic matrix, with the aim of comparing the main properties of the film containing nanosized ungrafted reinforcements in the same amount. In details, PLA nanocomposite containing silver grafted cellulose nanocrystals (PLA/0.5Ag-g-1CNC) was characterized by using UV-Vis, DSC, TGA analysis and the obtained results were compared with PLA nanocomposites containing 1%wt of pristine CNC (PLA/1CNC), 0.5% wt of silver

nanoparticles (PLA/0.5Ag) and hybrid system containing CNC and silver in the same amount (PLA/1CNC/0.5Ag). The antibacterial activity of the different systems was also studied.

2. Experimental part

Microcrystalline cellulose (MCC, dimensions of 10–15 μm), silver nitrate ($AgNO_3$), cetyltrimethylammonium bromide (CTAB) and sodium borohydride ($NaBH_4$) were supplied by Sigma–Aldrich® and used as received. All chemicals used in the experiment were analytic reagent. Silver nanoparticles were prepared by reducing the silver nitrate in CTAB aqueous solution, and $NaBH_4$ was used as a reducing agent. Poly (lactic acid) (PLA 3251D - specific gravity of 1.24 g/cm^3 and melt flow index of 6 g/10 min (210 °C, 2.16 kg)) was supplied by NatureWorks LLC, USA.

2.1 Preparation of CTAB mediated synthesis of Ag nanoparticles on cellulose nanocrystals

Cellulose nanocrystal (CNC) suspension was prepared from microcrystalline cellulose (MCC) by sulphuric acid hydrolysis (Fortunati et al., 2012a).

A multistep process was instead used to synthesize metallic nanoparticles: the Ag nanoparticles were synthesized via the conventional reduction of $AgNO_3$, CTAB acting as a nanoparticle stabilizer. Firstly, 0.3 mL of CTAB (0.5 mM) were added to the tube and stirred for 5 min, then 0.3 mL of $AgNO_3$ solution (100 mM) (pH 4.5-8.5) was added and allowed to react for 5 min; after that, 0.3 mL of the reducing agent sodium borohydride ($NaBH_4$) (0.03 wt %) was added to the suspension and held for 5 min, the solution was then washed with distilled water and dried in oven at room temperature. The Ag NPs on CNC templates by CTAB intermediate (Ag NPs-grafted-CNC) were then synthetized by following the paper of Padalkar et al. (Padalkar et al., 2010) (**Figure 1a**): CTAB was added to the CNC suspension (ca. 2 wt. % in DI water at pH~2) and allowed to react, then the metallic precursor solution (100 mM $AgNO_3$ (pH 4.5-8.5)) was added to

the CNC suspension; after that, ($NaBH_4$) (0.03 wt. %) was added to the suspension and held for 5 min, the solution was then washed with distilled water and freeze dried. The change in colour from white into yellowish brown of pristine cellulose nanocrystal and Ag grafted cellulose nanocrystal water solutions indicates that the grafting of AgNPs on CNC structure upon reduction was effective.

2.2 Preparation of PLA based nanocomposite films

PLA nanobiocomposite films were prepared by solvent casting method. PLA (2 g) was dissolved in 20 mL of chloroform ($CHCl_3$) with vigorous stirring at room temperature. For the preparation of the PLA/1CNC nanobiocomposite films, a predetermined amount of CNC suspension in chloroform was mixed with the previously prepared PLA solution. In the case of PLA/1CNC/0.5Ag, a predetermined amount of AgNPs dispersion in $CHCl_3$ was added to a solution prepared as described above for PLA/1CNC, after that this solution was stirred for another 2 h before they were cast onto the glass Petri dish. They were saved in dark medium. For the preparation of the PLA/0.5Ag-g-1CNC nanobiocomposite films, a predetermined amount of freeze dried silver grafted CNC was mixed with PLA solution. They were cast onto the glass Petri dish in dark medium (**Figure 1b)**.

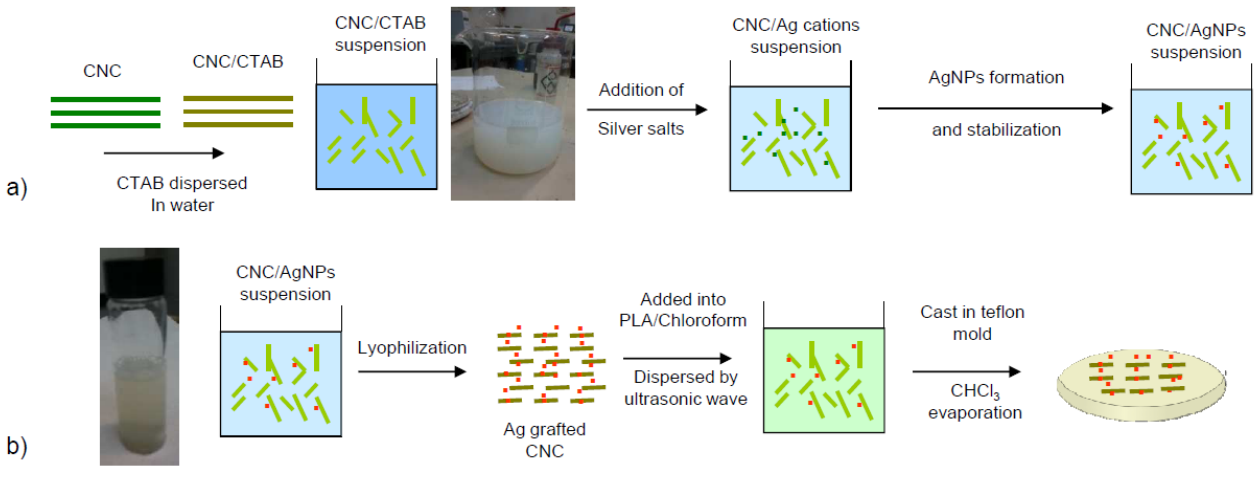

Figure 1: (a) Scheme of different preparation steps for CTAB mediated synthesis of Ag nanoparticles on cellulose nanocrystals (images of CTAB modified CNC and Ag-*g*-CNC water based solutions inserted) and (b) PLA nanocomposite films containing Ag-*g*-CNC.

2.3 Characterization of CTAB mediated synthesis of Ag nanoparticles on CNC

Characterizations of the CNC and Ag grafted CNC were achieved by different techniques. X-ray diffraction (XRD) data were taken with a Philips Analytical X'Pert X-diffractometer (Philips Co., Netherlands), with Cu-Kα radiation (λ = 1.54056 A°). The data were collected from 2θ = 10–70° with a step interval of 1°. The microstructure of neat Ag NPs and Ag grafted CNC samples was investigated by using a scanning electron microscope, FESEM, Supra 25- Zeiss, Germany. The electrokinetic properties of neat CNC and Ag grafted CNC samples were determined by measuring the zeta-potential of particles with a Zeta-Meter 3.0+ (with a Zeiss DR microscope, GT-2 type quartz cell, molybdenum-cylinder anode, and platinum-rod cathode electrode). The samples were stirred overnight in the deionized water to obtain well dispersed particles. The zeta potential of the dispersions was estimated from the measured electrophoretic mobilities by employing the Smoluchowski equation (Saka & Guler, 2006). In electrophoresis, the particles are moved by applying an electric field across the system. The electrophoretic mobility of neat CNC and Ag grafted CNC were analyzed for both directions of the applied electric field. The value of the zeta potential assigned to the dispersions was the average of the data obtained from at least 10 experiments. The applied voltage during the measurements was varied in the range 30–40 mV. The electrokinetic charge densities were also calculated according to equations in our previous study (Yalcinkaya & Guler, 2010).

2.4 Characterization of PLA based nanocomposite films

DSC (TA Instrument, Q200) measurements were performed in the temperature range from -25 to 210 °C at 10 °C/min under nitrogen flow; PLA and PLA nanocomposite samples (6–7 mg) were heated from -25 to 210 °C at a rate of 10°C/min and held at 210 ◦C for 2 min to erase the thermal history (1^{st} scan), then they were cooled to -25 at 10 ◦C/min and reheated under the same conditions

153 (2^{nd}scan). Glass transition, cold crystallization and melting temperatures (T_g, T_{cc} and T_m) were
154 determined from the first and second heating scans.
155 TGA was carried out by using a thermogravimetric analyzer (TGA, Seiko Exstar 6300). The
156 samples, approximately 8 mg, were heated from 30 to 900 ˚C at a heating rate of 10 ˚C/min under
157 nitrogen atmosphere. The weight-loss rate was obtained from derivative thermogravimetric (DTG)
158 data.
159 The microstructure of PLA nanocomposite films was investigated by scanning electron microscope,
160 FESEM, Supra 25-Zeiss. For fracture analysis, brittleness was enhanced using liquid nitrogen, then
161 the fracture sections of the nanocomposites were analyzed following gold sputtering of the samples.
162 In order to investigate the optical properties of the produced nanocomposites, spectroscopic analysis
163 for neat PLA and PLA nanocomposites was performed by means of a UV–Vis instrument (Perkin
164 Elmer Instruments (Lambda 35)), working in the wavelength between 250 and 900 nm.
165
166 ***2.5 Antibacterial assays***
167 *2.5.1 Bacterial strain culture conditions and viability assays.*
168 *Escherichia coli* RB (*E. coli* RB) and *Staphylococcus aureus* 8325-4 (*S. aureus* 8325-4) were used
169 in this study as main representatives of Gram negative and Gram positive bacteria, respectively. *E.*
170 *coli* RB was kindly provided by the "Istituto Zooprofilattico di Pavia", Italy whereas *S. aureus*
171 8325-4 was generously supplied by Timothy J. Foster (Department of Microbiology, Dublin,
172 Ireland). *E. coli* RB was routinely grown in Luria Bertani Broth (LB) (Difco, Detroit, MI, USA) and
173 *S. aureus* 8325-4 in Brian Heart Infusion (BHI) (Difco) overnight under aerobic conditions at 37◦C,
174 250 rpm (Certomat® BS-T, B.Braun Biotech International). To evaluate the antimicrobial activity of
175 PLA and PLA nanocomposite films enriched with different Ag preparations, the overnight cultures
176 were diluted in fresh appropriate medium and 200µl of diluted bacterial suspension were deposited
177 on sterilized PLA nanocomposites film discs placed at the bottom of a 96-well flat-bottom

polystyrene tissue culture plates (TCPs) well. 5 x 10^4, 5 x 10^3 and 5 x 10^2 cells/ml suspensions, obtained by comparing the OD_{600} of the overnight culture with a standard curve correlating OD_{600} to cell number, were used to test the antibacterical activity at 3, 6 and 24 hours of incubations, respectively. The TCP was then incubated at either 37°C or +4°C for 3, 6 or 24 hours in static conditions. Furthermore, three wells of TCP, used as controls, were inoculated at the same temperatures, times and with the same amount of diluted bacterial suspension. These temperatures were chosen to evaluate their influence on the antibacterial activity exerted by PLA and PLA nano-biocomposite films as food packaging systems. Some food is kept refrigerated at +4°C but it may be possible that under transportation food could be kept at higher storage temperatures (up to 37°C).

At the end of the culturing period, the bacterial viability was assayed through the quantitative 3-[4,5-dimethylthiazol-2-yl]-2,5diphenyltetrazoliumbromide (MTT) (Sigma Aldrich, StLouis, MO, USA) test (Cochis et al., 2016). This colorimetric assay measures dehydrogenase activity, as an indicator of the metabolic state of the cells. After the indicated culturing times, bacterial suspensions were transferred to a new plate and viability assessed. 5 mg/mL of MTT solution, dissolved in PBS (0.134 M NaCl, 20mM Na_2HPO_4, 20 mM NaH_2PO_4), was used as stock solution and the working concentration was 0.5mg/mL. Bacteria were incubated in the presence of MTT solution at 37°C for 3 hours. Upon presence of viable cells, reduction of MTT salt results in purple insoluble formazan granules. These precipitates are dissolved through acidified 2-propanol (0,04 N HCl). The result was recorded through an iMark® Microplate Absorbance Reader (Bio-Rad) at 562nm with the reference wavelength set at 655nm. Cell survival was expressed as percentage of the number of bacteria survived on PLA nano-biocomposite Ag-enriched films to number of bacteria grown on PLA neat films. Experiments were conducted in duplicate.

2.5.2 Inductively coupled plasma mass spectrometry (ICP-MS). To determine the release of Ag^+, PLA nanocomposite films of the area 1 cm^2 were incubated in bi-distilled sterile water either at 37°C or +4°C for 2 different incubation times (3 and 24 hours). The realeas of Ag cation was assessed with a Perkin-Elmer series ICP-MS, analysing those solutions obtained after the incubation times as indicated above. Sample solutions were regularly analyzed by ICP-MS to determine the concentration of Ag^+, once the instrument was calibrated with a standard solution.

2.5.3 Agar disc diffusion tests. To qualitatively assess the antimicrobial efficacy of the generated Ag-enriched PLA nanobiocomposites, agar disc diffusion tests were performed as previously described (Zare et al., 2014). Briefly, bacteria were cultured over night as described in Experimental part Section 2.5.1 and reduced to final density of 10^8 cfu mL^{-1} prior to inoculation of plates. Muller–Hinton agar (Difco) plates were prepared and inoculated from the standardized cultures uniformly spreading bacteria throughout the entire plate. In order to verify effects both in direct and indirect conditions, either sterilized PLA nanocomposites or sterile paper discs (6 mm diameter, Oxoid) soaked with 25 µL of the sterile water incubated 24 hours at 37°C in contanct with Ag-enriched PLA films were respectively used to determine inhibition growth. Disks were layed on the upper part of the seeded agar plate and incubated at 37°C for 24 hours. The antibacterial activities of the compounds were compared with 30% H_2O_2 (25 µL/disk) as positive control. Antibacterial activity was evaluated by measuring the diameter of inhibition zone (mm) on the surface of plates and the results were reported as Mean ± SD after three repeats.

2.5.4 Scanning electron microscopy (SEM). Images of *E. coli* RB and *S. aureus* 8325-4 grown on PLA films were prepared essentially as already reported (Fortunati et al., 2013b). Briefly, both strains used in this study were incubated on previously sterilized PLA film discs for 24 hours at

37°C. Following incubation, samples were washed carefully with sterile water and fixed with 2.5% (v/v) glutaraldehyde in 0.1 M Na-cacodylate buffer, pH 7.2, for 1 h at +4 °C. After additional washing with cacodylate buffer to remove the excess of glutaraldehyde, the samples were dehydrated using increasing concentrations of ethanol (25, 50, 75%) for 5 min and final two washes of 10 minutes in 96% ethanol. The samples were then lyophilized for 3 hours using an Emitech K-850 apparatus and placed on a mounting base. Finally, PLA discs were sputter coated with gold (300 nm) and investigated using a Zeiss EVO-MA10 scanning electron microscope (Carl Zeiss, Oberkochen, Germany).

2.6 Statistics

Each experiment reported in the results section was done in triplicates and at least in 2/3 separated experiments. Results are expressed as the mean ± standard deviation. In order to compare the results with the PLA reference, a two-way ANOVA with Bonferroni post-test was applied, with a significance level of 0.05.

3. Results and Discussion

3.1. Characterization of synthesized silver and cellulosic based nanoparticles

Figure 2a shows a FESEM image of cellulose nanocrystals, isolated from microcrystalline cellulose by acid hydrolysis, after CTAB modification, while in the inset the typical morphology of pristine CNC is reported. The unmodified nanocrystals presents the typical acicular structure with dimensions ranging from 100 to 200 nm in length and 5–10 nm in width (Fortunati et al., 2012b). After modification with CTAB, CNC maintain their shape and dimensions although appeared more individualized.

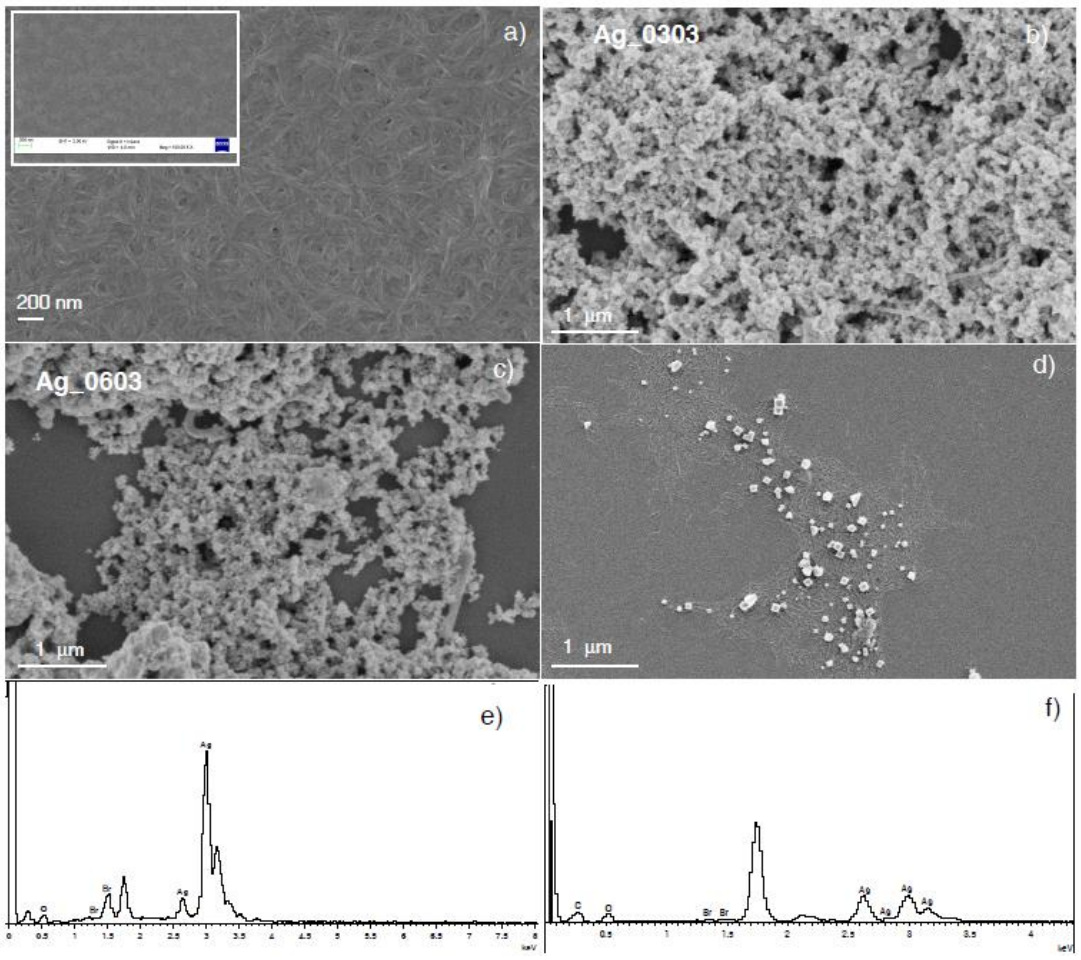

Figure 2. FESEM images of CTAB modified CNC (CNC in the inset) (a), neat AgNP samples obtained by using different $AgNO_3$ salt solution concentrations: (b) 0.03 mmol $AgNO_3$ and (c) 0.06 mmol $AgNO_3$. EDX spectrum of Ag (e) and Ag-*g*-CNC nanoparticles (f).

Parallely, neat Ag nanoparticles were synthesized via the conventional reduction of $AgNO_3$, by using CTAB as nanoparticle stabilizer, and changing the amount of $NaBH_4$ reducing agent. As reported in the literature, surfactants have been used by chemists and materials scientists as template systems for the stabilization of various types of nanocrystals and nanostructures. CTAB is a cationic surfactant that assembles into micelles in aqueous solution, previously successfully used to stabilize inorganic nanoparticles (Cai et al., 2009; Sun et al., 2002). The stabilized nanoparticles, which are covered in polar cationic quaternary ammonium groups, can then no covalently interact with other polar surfaces (as in the case of CNC nanocrystals, which are rich in free hydroxyl groups). In the synthesis of CTAB stabilized Ag nanoparticles, we observed that less

agglomeration and reduced dimensions for nanoparticles were obtained when lower amount of silver nitrate (Ag_0303) is considered in the reaction, in comparison with Ag_0603 sample, with double amount of salt (**Table 1**). FESEM images of neat Ag NP samples synthesized with these two different $AgNO_3$ salt solution concentrations (0.03 mmol $AgNO_3$ and 0.06 mmol of $AgNO_3$) are reported in **Figure 2b** and **2c**, respectively. According to the literature, high pH values also resulted in a large amount of unspecific silver deposition on the substrate (Sun et al., 2008), while it has been reported that, in basic conditions, aggregation of Ag nanoparticles obtained by surfactant stabilization and $NaBH_4$ reduction occurs. This effect can be attributed to hydrophobic interactions between uncharged CTAB molecules at slightly basic pH, rendering them insoluble (i.e., unable to stabilize and prevent Ag nanoparticle aggregation). In our case, the pH of $AgNO_3$ solution was kept constant at 6.5.

Experimental conditions for synthesis of Ag and Ag-*g*-CNC nanoparticles were also set up considering different parameters, such as salt and reducing agent amounts, reaction time at a fixed content of CNC (2% wt.). **Figure 2d** reports the obtained morphology of Ag-*g*-CNC nanoparticles resulting from conditions considered in Table 1 for sample G (Ag-*g*-CNC_06_1.0_120). In order to validate that AgNPs correctly formed on CNC, SEM-EDX analysis was performed and their approximate bulk atomic composition was investigated. SEM-EDX spectra of Ag and Ag-*g*-CNC are shown in **Figure 2e** and **Figure 2f**, respectively. The obtained EDX spectrum for Ag-*g*-CNC confirmed the existence of silver onto CNC. This observation indicates that Ag ions quantitatively deposited on CNC surface (hydroxyl groups) followed by reduction with $NaBH_4$.

Table 1: Experimental conditions for synthesis of Ag and Ag-*g*-CNC nanoparticles

Sample	**$AgNO_3$ (100mM)** (mL)	**$NaBH_4$ (0.03% wt)** (mL)	**CTAB (0.5mM)** (mL)	**CNC (2%wt)** (mL)	**time** (min)
Ag_0303	0.3	0.3	0.3		30
Ag_0603	0.6	0.3	0.3		30

A (Ag-*g*-CNC_03_03_30)	0.3	0.3	0.3	1	30
B (Ag-*g*-CNC_06_03_30)	0.6	0.3	0.3	1	30
C (Ag-*g*-CNC_06_03_60)	0.6	0.3	0.3	1	60
D (Ag-*g*-CNC_06_06_60)	0.6	0.6	0.3	1	60
E (Ag-*g*-CNC_06_06_120)	0.6	0.6	0.3	1	120
F (Ag-*g*-CNC_06_1.0_60)	0.6	1	0.3	1	60
G (Ag-*g*-CNC_06_1.0_120)	0.6	1	0.3	1	120

(Ag-g-CNC_x_y_z), where x and y represent AgNO3 and NaBH4 amounts, respectively, while z is the reaction time

This morphology observed in Figure 2d was the result of an optimized procedure, in which the influence of $NaBH_4$ amount and reducing time was monitored. In order to determine the optimum amount of $NaBH_4$, Ag^+ ions, and CNC (if needed), the "one factor at a time" method was employed. This experiment design implied that one experimental factor was varied at a time, keeping the other factors constant. A comparison of previous experimental results obtained from the synthesis of AgNPs with these data let us to deduce that, as expected, the silver salt content was the crucial factor for the production of these nanoparticles. We observed that the reaction did not occur completely for the lower selected content of AgNO3, (sample A in Table 1, Ag-*g*-CNC_03_03_30) (**Figure 3a, Panel A**), while with increasing amount (sample B, Ag-*g*-CNC_06_03_30) AgNPs were synthesized on CNC surface (**Figure 3b, Panel A**).

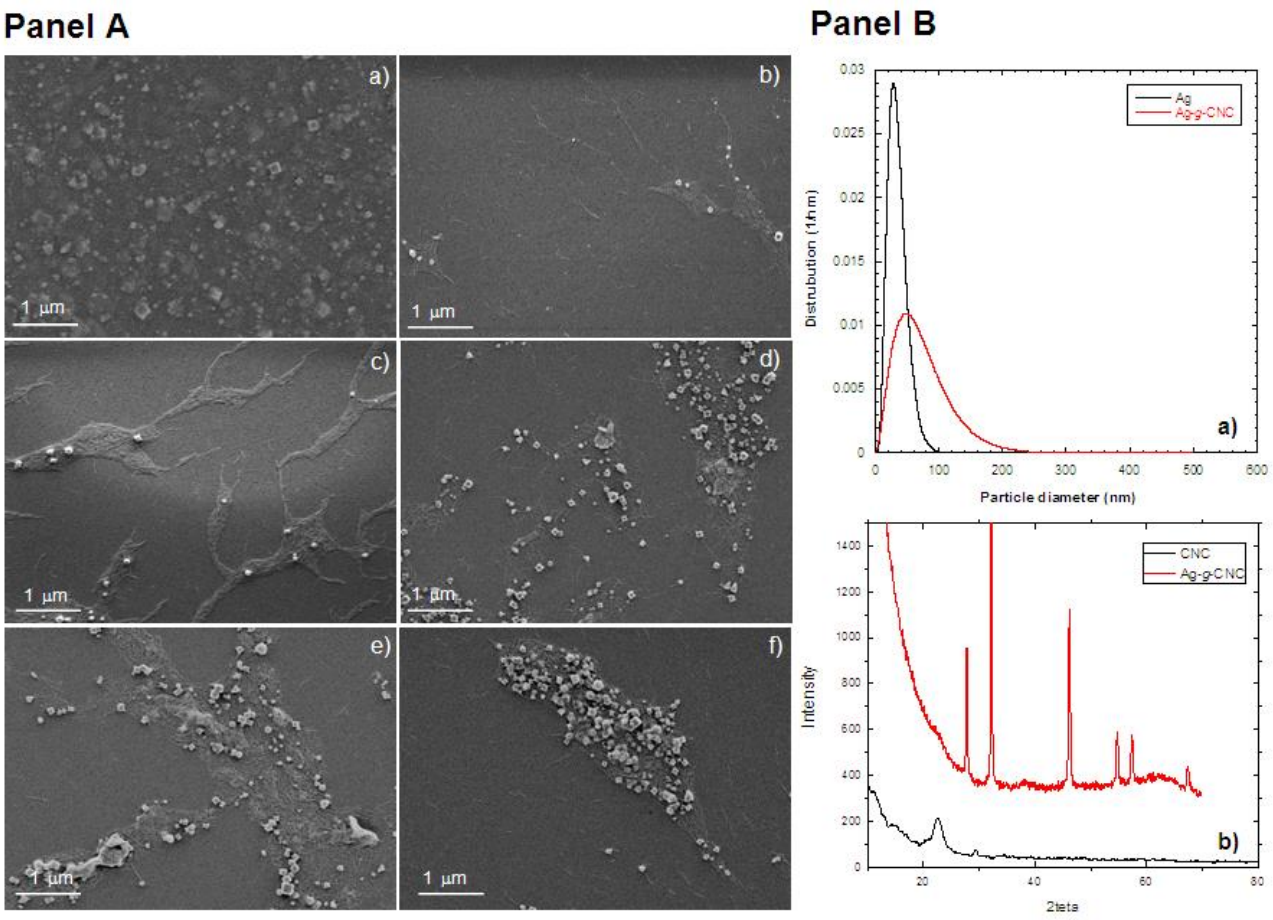

Figure 3: (Panel A, from a to f): FESEM images of Ag-*g*-CNC powders with varying concentration of $NaBH_4$ and varying reaction times 120 min; (Panel B) particle size distribution for neat Ag and Ag-*g*-CNC nanoparticles (a) and XRD patterns of the neat CNC and Ag-*g*-CNC nanoparticles (b).

Once fixed the silver salt concentration, we varied both the reaction time at 60 min (sample C, Ag-*g*-CNC_06_03_60, **Figure 3c, Panel A**) and the reducing agent concentration (sample D, Ag-*g*-CNC_06_06_60, **Figure 3d, Panel A**). Also in this case we observed that grafting was more effective when higher amount of reducing agent were considered, so we decided tyo study the process by taking fixed the amount of silver salt and reducing agent at 0.6. After that, a different reaction time was considered (120 min) and we observed that, with prolonged reaction time, the average Ag particle size increased from ~17 nm in the case of 60 min (measurements taken from FESEM images (sample D, Ag-g-CNC_06_06_60) up to ~36 nm in the case of 120 min (sample E, Ag-g-CNC_06_06_120, **Figure 3e, Panel A**). Approaching the process varying again the reducing agent

content at this optimized conditions and reaction time, sample F (Ag-g-CNC_06_1.0_60, **Figure 3f, Panel A)** and sample G (Ag-g-CNC_06_01_120, **Figure 2d**) morphologies were obtained. These obtained results confirmed us that mean diameters of the AgNPs gradually increases with increased value of reaction time at a constant temperature and the best compromise in terms of reaction efficiency for Ag synthesys on CNC surfaces and particles dimensions can be obtained with high reducing agent content (1mL) and lower reaction time (60 min) (sample F, Figure 3f).

Power X-ray diffraction patterns of pristine CNC and Ag-*g*-CNC were also presented in **Figure 3a, Panel B**. The diffraction pattern for neat CNC showed intense peak at 15°, 16°, 22°, 29°, and 34°, that are the characteristic peaks of CNC (Drogat et al., 2011): these peaks represented the typical cellulose-I structure, with cellulose crystals exhibiting characteristic assignments of 110, 200, and 004 planes, respectively (Wada, Heux & Sugiyama, 2004; Park et al., 2010). XRD pattern for Ag-*g*-CNC showed additional peaks at 32°, 46°, 54°, 57° and 67° which are assigned to (111), (200), (220), and (311) crystallographic planes of cubic silver (Das et al., 2009). Crystallite size of the silver nanoparticles was calculated by using full width at half maximum (FWHM) of the 100% peak of silver and the Scherrer's formula (Eq. 1):

$$d = K\lambda/(\beta \cdot cos\theta) \qquad (1)$$

where d is the average particle size, λ is X-ray wavelength, β is FWHM of the diffraction line, θ the diffraction angle, and K constant, generally assumed as 0.9. The calculated average particle size of neat AgNPs is about 30 nm (**Figure 3b, Panel B**), nevertheless the average particle size of Ag-*g*-CNC was about 50 nm. This indicates that the grafted Ag-*g*-CNC tend to form large clusters which it is consistent with the inherent aggregation characteristics of AgNPs (Sharma et al., 2014).

The zeta potential result is an indicator of the surface charge properties of a colloid or a particle in solution and varies depending on the surface potential and the thickness of the electric double layer. It is usually characterized by the measurement of the electrophoretic mobility of the colloidal

particles in dispersion which is a key technique for the determination of the stability of the particles (Yalcinkaya & Guler, 2010). The zeta potential is also an important parameter for a number of applications including characterization of biomedical polymers, electrokinetic transport of particles or blood cells, sensors and biosensors, membrane efficiency and microfluidics (Bauman et al., 2013). In this study, the pristine CNC had a strongly negative charge in water as evidenced by a zeta potential measured value of approximately -45 ±1.24 mV. After grafting of the Ag nanoparticles, the zeta potential was measured as -27.5±0.73 mV. After each grafting step, the zeta potentials shifted to less negative values as a result of adsorption of positively charged silver particles at the surface of CNC. This result was supported by electrokinetic charge densities, that were calculated as -29×10^{-3} and -19.2×10^{-3} Cm^{-2} for CNC and Ag-*g*-CNC, respectively.

3.2. Characterization of PLA based nanocomposite films

The adopted Ag grafting procedure suggested us to incorporate these modified nanoparticles in polymeric films, in order to test how the main thermal, morphological and antibacterial properties of the produced materials could be affected by the presence of Ag-*g*-CNC with respect of neat Ag nanoparticles synthesized by using CTAB intermediate. The absorption and transmission of light by polymer films is an important property in many industrial applications, as in the food packaging industry, where the packaged goods are light sensitive (Turhan & Sahbaz, 2001).. In the fresh food packaging, an important issue is the effect of irradiation in the package, since ultraviolet light irradiation is a common method used for lowering microbial population in foods. The spectrum and the intensity of the light source, the conditions of light exposure, and the degree of light transmittance of the packaging material are factors that can dramatically affect the food quality. The results from the UV–Vis characterization for films produced by incorporating pristine CNC and/or Ag nanoparticles and Ag-*g*-CNC in PLA matrix by means of a solvent casting approach, are shown in **Figure 4a**. The nanocomposite formulations showed optical properties similar to the neat PLA

film, without a significant reduction in the amount of reflected light in a wide range of Vis region (region above 500 nm), documenting the good transparency of the produced nanocomposite films.

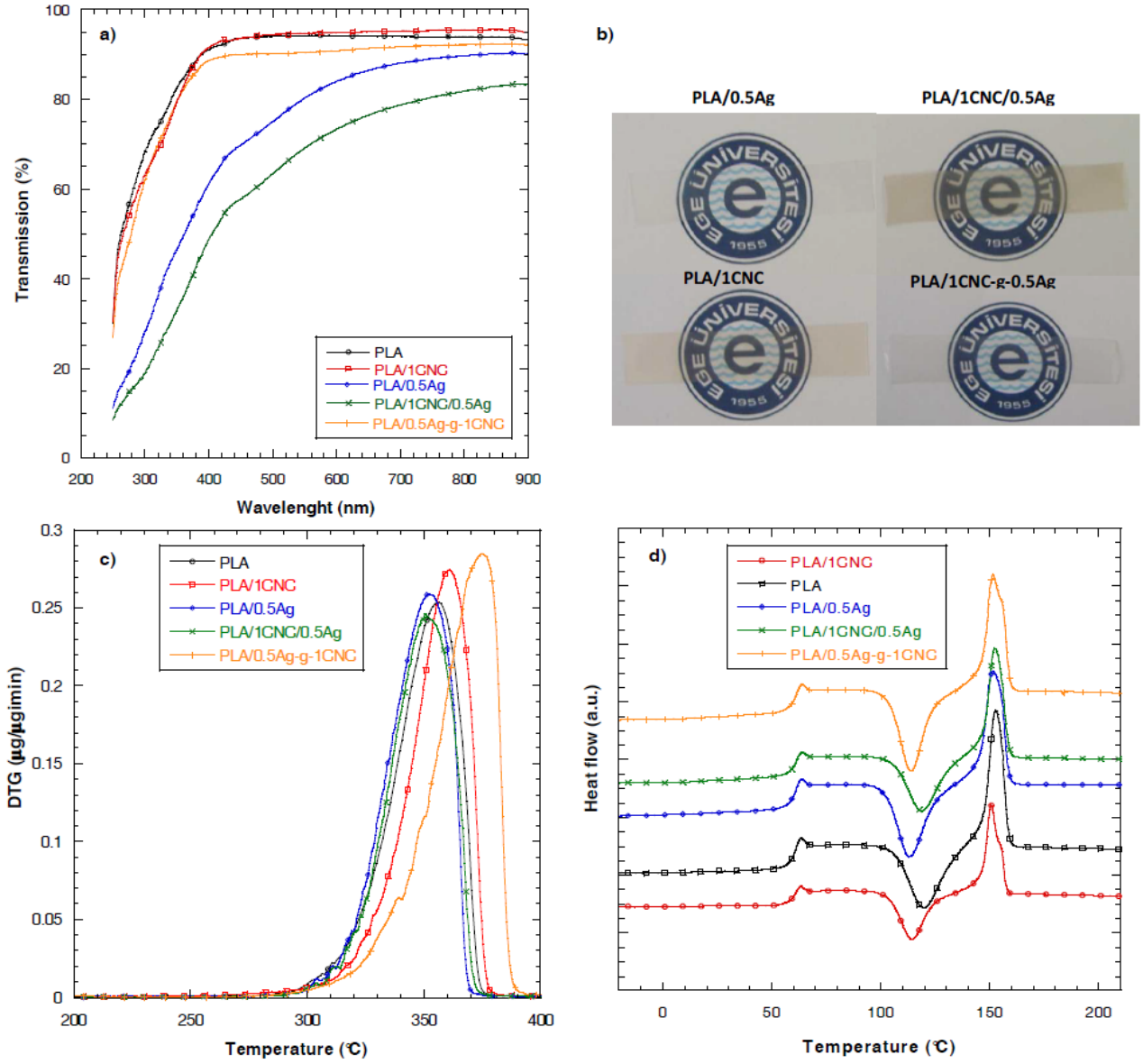

Figure 4: UV-Vis spectra (a), images of transparent films based on PLA and different reinforcements (b), DTG curves (c) and DSC (d) thermograms (first heating scan) of neat PLA and different PLA nanocomposite films containing CNC and AgNPs.

However, some yellowing was observed in the case of formulations containing silver nanoparticles. In particular, in the 800-500 nm range and below 250 nm all the films showed similar spectra, overlapping, within the experimental error, with the spectrum of neat PLA. Lower light reflection intensities were detected for all the nanocomposite samples containing ungrafted AgNPs, and this

behaviour is likely due to the light extinction due to the presence of silver nanoparticles (Baia et al., 2007). As expected, a reduction in the amount of transmitted light was observed for PLA/0.5Ag and PLA/1CNC/0.5Ag systems containing unmodified silver nanoparticles, in comparison with neat PLA and PLA/1CNC (for which the introduction of 1% wt. of CNC did not affect the property). At 500 nm, a light transmission value of 95% was measured for neat PLA, while in the case of PLA/0.5Ag and PLA/1CNC/0.5Ag films, values of 85% and 80% were detected, respectively. Unexpectedly, the PLA/Ag-*g*-CNC film has similar light transmission of neat PLA system. Images from **Figure 4b** confirmed the transparency of PLA/Ag-*g*-CNC film.

Thermal behaviour of pristine PLA and different PLA nanocomposite films was investigated and the results from TGA analysis are reported in **Figure 4c** (DTG curves). A complete weight loss in a single step with a maximum at 358 ^{o}C was detected for neat PLA. A similar behaviour was found for PLA/0.5Ag and PLA/0.5Ag/1CNC; a single degradation step between 300 and 400 ^{o}C, with a maximum at about 358 ^{o}C is occurred, corresponding to the thermal decomposition process of the polymer. This result indicated that the introduction of 0.5%wt of unmodified silver nanoparticles or 1%wt of CNC did not influence the matrix thermal degradation. However, in the PLA/1CNC nanocomposite, a shift to higher temperatures of about 10^{o}C in T_{max} value was observed, while a further increase of about 30 ^{o}C was detected for the PLA/Ag-*g*-CNC nanocomposite, indicating that grafting of silver nanoparticles on cellulose nanocrystals positively affected the thermal stability of the final nanocomposite formulations. DSC analysis was also performed to investigate the glass transition, crystallization and melting phenomena of PLA and its nanocomposite films in relation to the composition. The glass transition temperatures and melting phenomena of the nanocomposites did not change significantly respect to the PLA polymer matrix during the first heating scan (**Figure 4d**). The cold crystallization temperature showed a shift to lower temperature of about 7°C when CNC and AgNPs were introduced separately (PLA/0.5Ag and PLA/1CNC binary systems): this result suggests a good dispersion in the case of CNC and AgNPs, since well dispersed nanofillers

are able to promote the cold crystallization at lower temperatures (Fortunati et al., 2012a). A more intense T_{cc} peak was detected in the case of PLA/0.5Ag-*g*-1CNC nanocomposite, that has shown the same crystallization behaviour, in terms of temperatures, respect to the neat system, suggesting that the fillers were able to promote PLA nucleation.

The antibacterial effect of PLA neat film and the generated PLA nanocomposites enriched with silver nanoparticles was investigated by using two different bacterial strains: *Escherichia coli* RB and *Staphylococcus aureus* 8325-4, representative of Gram-negative and Gram-positive classes, respectively. We investigated bacterial survival over a range of incubation times (3, 6 and 24 hours) at two temperatures (+4°C and 37°C) for both the selected strains (**Figure 5**).

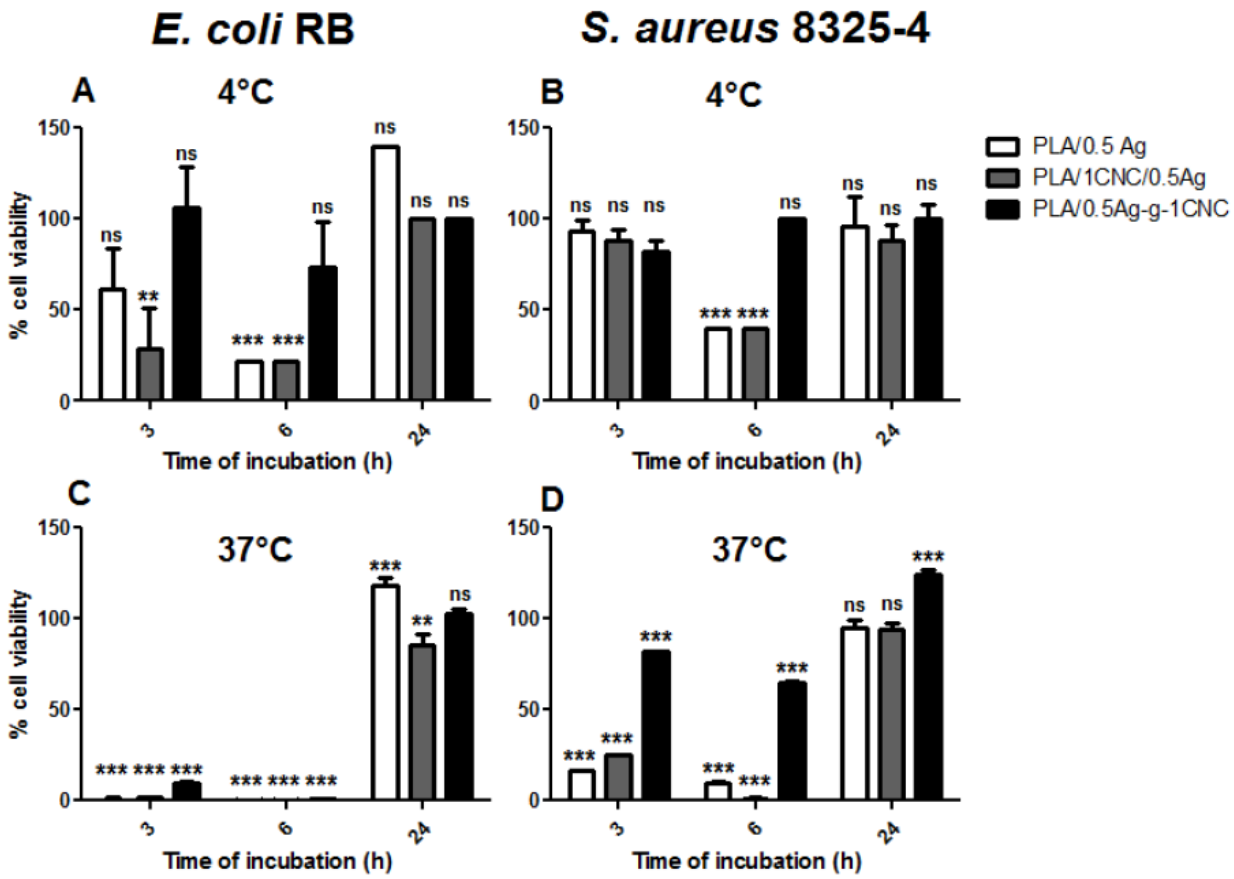

Figure 5. Cell viability of *E. coli* strain RB (A and C) and *S. aureus* strain 8325-4 (B and D) on different PLA nanocomposites at two temperatures (+4°C and 37°C) and three different incubation times (3, 6 and 24 h). Data are presented as viability percentage to PLA set equal to 100%. Two-way ANOVA with Bonferroni post-test was performed to evaluate statistical significance. All data were compared with PLA reference (**=p<0.01***=p<0.001, ns= p>0.05)

Bacterial viability was also tested on TCPs and compared to PLA neat film: the results showed to be similar with no significant differences ($p > 0.05$) (data not shown). Data are presented using PLA plain film as a reference set at 100% of bacterial viability. Commonly, the effect of Ag on bacterial viability was more evident at 37°C rather than at +4°C. Furthermore, as expected, *E.coli* survivability was more affected by the presence of silver in the nanomaterials if compared to *S. aureus*. The structural differences of the cell wall among Gram-positive and Gram-negative bacteria mainly account for the different efficacy of Ag (Feng et al., 2000). Gram-positive bacteria are characterized by a thick layer of murein that hampers the access of Ag^+ ions to the bacterial cell. On the contrary, an outer membrane and a less thick layer of peptidoglycan surround Gram-negative bacteria. The outer membrane of these bacteria is characterized by the presence of General Bacteria Porins (GBP), that are β-barrel proteins that are thought to mediate an energy-indipendent acces of metal ions to Gram-negative cell membrane (Lemire et al., 2013). Thanks to the permeability of these channels, metal ions have much easier access to plasma membrane and to the cell. In fact, the mechanistic base of Ag damage is then similar between the two bacterial classes, once the contact is made with plasma membrane. Ag^+ ions mediate ruffling of the membrane and immediately interact with thiol groups and Fe-S clusters of exposed proteins. Among these proteins are respiratory chain components that become easily inactivated and start to de-energize the bacterial cell, leading to the death of the bacterium. Once Ag has disrupted plasma membrane, it gains access to cytoplasmatic proteins and bacterial DNA. The former are again affected at thiol groups, instead genomic DNA turns to a condensed form that is no more able to undergo proper replication and transcription (Mijnendonckx et al., 2013). Therefore, the antibacterial effect of silver ions is dependent on the accessibility of bacterial plasma membrane. Our results indicated that *E.coli* growth is inhibited to an undetectable level when cultured at 37°C for 3 and 6 hours for all nanocomposites films, except for PLA/0.5Ag-*g*-1CNC at 3 hours whose growth was still significantly reduced ($p < 0.001$) but detectable (**Figure 5C**). By contrast, *S. aureus* (**Figure 5D**) did show a significantly reduced

viability ($p < 0.001$) when incubated for 3 and 6 hours at 37°C in contact with all Ag-enriched films, but the growth was still detectable. Interestingly, all bio-nanocomposites displayed a bacteriostatic effect at longer incubation times (24 hours) for both strains at 37°C. However, the growth of *E.coli* on PLA/1CNC/0.5Ag showed a slight inhibition of growth ($p < 0.01$). On all the other samples, the bacterial viability was comparable to PLA. The cell viability of both strains at +4°C was also assessed (**Figure 5A** and **Figure 5B**).

Mostly, the growth rates were lower due to the low temperature. Again, as expected, *E. coli* showed to be more susceptible to the presence of Ag than *S. aureus*. As already reported at 37°C, at longer incubation times (24 hours), all PLA nanocomposites proved to be bacteriostatics rather than bactericidal against both strains. At shorter incubation times, bactericidal effects were less evident when compared to the corresponding conditions at 37°C. However, a significant reduction of *E. col*i growth was detected on PLA/1CNC/0.5Ag at both 3 and 6 hours ($p < 0.01$ and $p < 0.001$, respectively). PLA/0.5Ag exhibited a significant reduction of growth at 6 hours ($p < 0.01$), but not at 3 hours ($p > 0.05$). At these two time intervals, PLA/0.5Ag-g-1CNC was not able to significantly reduce the growth of *E. coli* ($p > 0.05$). *S. aureus* instead was not affected by Ag presence at all incubation times on all PLA Ag-enriched films ($p > 0.05$), except at 6 hours. At this time interval, PLA/0.5Ag and PLA/1CNC/0.5Ag could inhibit staphylococcal growth to significantly lower extent ($p < 0.001$).

The general lower efficacy of PLA nanocomposites at low temperatures can be explained to the less efficient release of Ag^+. In fact, to correlate the antibacterial activity of the generated bio-nanocomposites, we analyzed the Ag^+ release through ICP-MS analysis under the same experimental conditions of the viability assays (**Table 2**). The release of Ag^+ ions at +4°C was one order of magnitude lower if compared at 37°C (ng/L vs µg/L).

Table 2: ICP measurement of Ag^+ release by different PLA based formulations following incubation in bidistilled water at two different times (3 and 24 hrs) and temperatures (+4°C and 37°C), respectively.

	4°C (ng/l)		**37°C (µg/l)**	
	3 hours	*24 hours*	*3 hours*	*24 hours*
PLA	0.01	3,00	0,01	0,01
PLA/0.5Ag	23,00	58,00	80,00	128,00
PLA/1CNC/0.5Ag	57,00	103,00	115,00	223,00
PLA/0.5Ag-g-1CNC	14,00	19,00	38,00	74,00

These data also allowed us to understand that the broad less efficient antibacterial effect displayed by PLA/0.5Ag-*g*-1CNC nanocomposite is essentially due to the lower Ag release, both at +4°C and 37°C. This can be due to the grafting procedure used to produce PLA/0.5Ag-*g*-1CNC. However, at 37°C, the Ag^+ release was more plentiful from PLA/0.5Ag and PLA/1CNC/0.5Ag at short incubation time, explaining the antibacterial efficiency on cell viability up to 6 hours for both strains; this antibacterial activity is reduced at 24 h as well as the amount of released Ag^+ except for the PLA/1CNC/0.5Ag samples that seems to show the best performance.

A similar trend, even if at a lower extent due to a reduced Ag^+ release, can explain the bacterial viability data obtained at +4°C at both short and long incubation times.

To visualize antimicrobial effects of the generated Ag-enriched PLA nanocomposites, SEM observations of *E. coli* and *S.aureus* grown for 24 h at 37°C on PLA and PLA nanocomposites were also performed. Agar disc diffusion tests were attempted but no positive results were recorded (data not shown) owing, we believe, to the extreme paucity of Ag released by the nanomaterials, as determined thanks to ICP-MS analysis. Thus, SEM investigation was exploited both to evaluate either the bacterial adherence to the tested materials and the effect exerted by the release of Ag^+ on the cell morphology of both strains (**Figure 6**).

The reason why we performed the SEM observations at higher temperature is due to the fact the Ag^+ release is too low at +4°C to justify this experimental set-up. In general, *E. coli* RB showed a reduced adherence to all films in comparison to *S. aureus* 8325-4. However, the gross morphology of both bacterial cells was normal and quite similar on all nanocomposites films. Taking into account antibacterial test and Ag-release analysis, we hypothesize that the vehicle of antimicrobial effect of the generated Ag-enriched PLA films is the direct contact of bacteria with the nanomaterial. The grafting procedure adopted to generate PLA/0.5Ag-g-1CNC might result in a surface where Ag is less available and more entrapped, thus resulting in a less efficient antimicrobial activity. Conversely, PLA/0.5Ag and PLA/1CNC/0.5Ag, where Ag nanoparticles did not undergo the grafting procedure, exerted better antibacterial properties owing to their more available Ag.

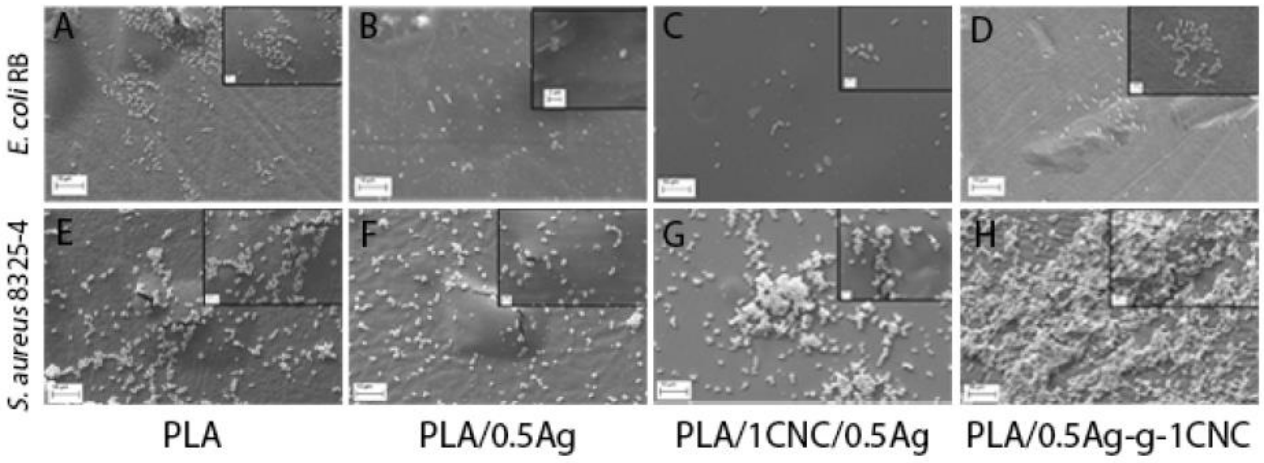

Figure 6: SEM rapresentative images of *E. coli* strain RB (panels A, B, C and D) and *S. aureus* strain 8325-4 (panels E, F, G and H) seeded on the different PLA materials and incubated for 24 hrs at 37°C.

The use of metallic ions as antimicrobial agents in different formulations has been extensively applied. For instance, the use and antibacterial effects of Ag, Ni, Zn, Cu are well known and mostly characterized, also at molecular level (Lemire et al., 2013). Recently also Fe has been employed in the generation of magnetic antibacterial nanoparticles either coupled to Ag or Au to target bacterial biofilms thanks to a external magnetic field (Mahmoudi & Serpooshan, 2012) or in combination

with other chemicals to form multilayered nanoparticles (Zare et al., 2015; Hasantabar et al., 2015). The use of metals as antimicrobials has great potential due to the tremendous increase in antibiotic resistence phenomena. Nevertheless, public issues owing to possible side effects upon environmental or direct exposure (e.g. upon incorporation in medical devices or for food packaging purposes) to these metals may represent a limit in their use (Lemire et al., 2013). Since our generated materials are intended for a food packaging approach, the fact that they both display good antibacterial properties and release small amount of Ag renders them suitable for their end use.

Summarizing, the PLA nanocomposite films produced in this study displayed a good antibacterial activity at short incubation intervals, especially at 37°C. At longer incubation times, they showed a bacteriostatic behavior at both the tested temperatures. Furthermore, PLA/0.5Ag and PLA/1CNC/0.5Ag proved to be more efficient than PLA/0.5Ag-*g*-1CNC in affecting bacterial growth, due to higher Ag^+ release at 37°C if compared to +4°C. In general, the antibacterial efficacy of all films was more evident on *E. coli* rather than on *S. aureus* strain.

4. Conclusions

Cetyltrimethylammonium bromide (CTAB) was used as stabilizer for silver nanoparticle synthesis on CNC surface via the conventional reduction of $AgNO_3$: less agglomeration and reduced dimensions for nanoparticles were obtained when lower amount of silver nitrate was considered in the reaction. Mean diameters of the AgNPs (30 nm) gradually increases with increased value of reaction time at a constant temperature even in the case of Ag-*g*-CNC (calculated as about 50 nm). Zeta potential measurements confirmed the shift to less negative values for Ag-*g*-CNC, as a result of adsorption of positively charged silver particles at the surface of CNC. PLA films containing Ag-*g*-CNC showed similar light transmission of neat PLA film, while a reduction in the amount of transmitted light was observed for PLA/0.5Ag and PLA/1CNC/0.5Ag systems containing pristine

530 silver nanoparticles. It was also demonstrated that grafting of silver nanoparticles on cellulose
531 nanocrystals positively affected the thermal degradation process and cold crystallization
532 processes. Results of antibacterial tests showed that PLA nanocomposite films displayed a good
533 antibacterial activity, more evident on *E. coli* rather than on *S. aureus* strain, at short incubation
534 intervals, especially at 37°C, where PLA/0.5Ag and PLA/1CNC/0.5Ag proved to be more efficient
535 than PLA/0.5Ag-*g*-1CNC in affecting bacterial growth, due to higher Ag+ release.

536

537 **References**

538 Baia, L., Muresan, D., Baia, M., Popp, J., Simon, S. (2007). Structural properties of silver
539 nanoclusters–phosphate glass composites. *Vibrational Spectroscopy, 43*, 313-318.

540 Bauman, M., Kosak, A., Lobnika, A., Petrinic, I., Luxbacher, T. (2013). Nanofiltration membranes
541 modified with alkoxysilanes: Surface characterization using zeta-potential. *Colloids and Surfaces*
542 *A: Physicochemical and Engineering Aspects*, 422, 110-117.

543 Cacciotti, I., Fortunati, E., Puglia, D., Kenny, J.M., & Nanni, F. (2014). Effect of silver
544 nanoparticles and cellulose nanocrystals on electrospun poly(lactic) acid mats: morphology, thermal
545 properties and mechanical behavior. *Carbohydrate Polymers*, 103, 22-31.

546 Cai, J., Kimura, S., Wada, M., Kuga, S. (2009). Nanoporous cellulose as metal nanoparticles
547 support. *Biomacromolecules*, *10*, 87–94.

548 Cochis, A., Azzimonti, B., Sorrentino, R., Della Valle, C., De Giglio, E., Bloise, N., Visai, L., Bruni,
549 .G, Cometa, S., Pezzoli, D., Candiani, G., Rimondini, L., Chiesa, R. (2016) Data in support of
550 Gallium (Ga(3+)) antibacterial activities to counteract E. coli and S. epidermidis biofilm formation
551 onto pro-osteointegrative titanium surfaces, *Data in Brief., 6,* 758-762.

552 Das, R., Nath, S.S., Chakdar, D., Gope, G., Bhattacharjee, R. (2009) Preparation of silver
553 nanoparticles and their characterization, *Journal of Nanotechnology, 5*, 1-6.

554 Drogat, N., Granet, R., Sol, V., Memmi, A., Saad, N., Klein Koerkamp, C., Bressollier, P.,
555 Krauszet, P. (2011) Antimicrobial silver nanoparticles generated on cellulose nanocrystals. *Journal*
556 *of Nanoparticle Research, 13(4),* 1557–1562.

557 Feng, Q.L., Wu, J., Chen, G.Q., Cui, F.Z., Kim, T.N., Kim, J.O. (2000) A mechanistic study of the
558 antibacterial effect of silver ions on Escherichia coli and Staphylococcus aureus. *Journal of*
559 *Biomedical Materials Research, 52(4)*, 662-668.

560 Fortunati, E., Armentano, I., Zhou, Q., Puglia, D., Terenzi, A., Berglund, L.A., Kenny, J.M. (2012a)
561 Microstructure and nonisothermal cold crystallization of PLA composites based on silver
562 nanoparticles and nanocrystalline cellulose. *Polymer Degradation and Stability, 97(10),* 2027-2036.
563 Fortunati. E., Armentano, I., Zhou, Q., Iannoni, A., Saino, E., Visai, L., Berglund, L.A., Kenny,
564 J.M. (2012b) Multifunctional bionanocomposite films of poly(lactic acid), cellulose nanocrystals
565 and silver nanoparticles. *Carbohydrate Polymers, 87,* 1596– 1605.
566 Fortunati, E., Peltzer, M., Armentano, I., Jiménez, A., Kenny, J.M. (2013) Combined effects of
567 cellulose nanocrystals and silver nanoparticles on the barrier and migration properties of PLA nano-
568 biocomposites *Journal of Food Engineering, 18(1),* 117–124.
569 Fortunati, E., Mattioli, S., Visai, L., Imbriani, M., Fierro, J.L., Kenny, J.M., Armentano, I. (2013)
570 Combined effects of Ag nanoparticles and oxygen plasma treatment on PLGA morphological,
571 chemical, and antibacterial properties. *Biomacromolecules, 14(3),* 626-636.
572 Fortunati, E., Rinaldi, S., Peltzer, M., Bloise, N., Visai, L., Armentano, I., Jiménez, A., Latterini, L.,
573 Kenny, J.M. (2014) Nano-biocomposite films with modified cellulose nanocrystals and synthesized
574 silver nanoparticles. *Carbohydrate Polymers, 101,* 1122–1133.
575 Hasantabar V., Lakouraj M.M., Zare E.N., Mohseni M. (2015) Innovative magnetic tri-layered
576 nanocomposites based on polyxanthone triazole, polypyrrole and iron oxide: synthesis,
577 characterization and investigation of the biological activities. *RSC Advances,(5),* 70186-70196
578 Lemire J.A., Harrison J.J., Turner R.J. (2013) Antimicrobial activity of metals: mechanisms,
579 molecular targets and applications. *Nature Reviews Microbiology, 11(6),* 371-384.
580 Liu, H., Wang, D., Song, Z., Shang, S. (2011) Preparation of silver nanoparticles on cellulose
581 nanocrystals and the application in electrochemical detection of DNA hybridization. *Cellulose, 18,*
582 67–74.
583 Lokanathan, A.R., Uddin, K.M.A., Rojas, O.J., Laine, J. (2014) Cellulose Nanocrystal-Mediated
584 Synthesis of Silver Nanoparticles: Role of Sulfate Groups in Nucleation Phenomena,
585 Biomacromolecules, 15, 373−379.
586 Mahmoudi M, Serpooshan V.(2012) Silver-coated engineered magnetic nanoparticles are promising
587 for the success in the fight against antibacterial resistance threat. *ACS Nano;6(3),*2656-2664.
588 Marques, P.A.A.P., Nogueira, H.I.S., Pinto, R. J. B., Neto, C.P. , Trindade, T. (2008). Silver-
589 bacterial cellulosic sponges as active SERS substrates, *Journal of Raman Spectroscopy, 39(4),* 439-
590 443.
591 Mijnendonckx, K., Leys, N., Mahillon, J., Silver, S., Van Houdt, R. (2013) Antimicrobial silver:
592 uses, toxicity and potential for resistance. *Biometals, 4,* 609-621.

593 Padalkar, S., Capadona, J.R., Rowan, S.J., Weder, C., Won, Y-H, Stanciu, L.A., Moon, R.J. (2010)
594 Natural biopolymers: novel templates for the synthesis of nanostructures. *Langmuir, 26,* 8497–
595 8502.
596 Park, S., Baker, J. O., Himmel, M. E., Parilla, P. A., Johnson, D. K. (2010). Cellulose crystallinity
597 index: measurement techniques and their impact on interpreting cellulase performance.
598 *Biotechnology for Biofuels, 3,* 10
599 Pinto, R. J. B., Marques, P. A. A. P., Neto, C., Trindade, T., Daina, S., Sadocco, P. (2009)
600 Antibacterial activity of nanocomposites of silver and bacterial or vegetable cellulosic fibers, *Acta*
601 *Biomaterialia, 5(6),* 2279-2289.
602 Saka, E. E., Guler, C. (2006) The effects of electrolyte concentration, ion species and pH on the zeta
603 potential and electrokinetic charge density of montmorillonite, *Clay Minerals, 41(4),* 853-861.
604 Sharma, V. K. K., Siskova, M., Zboril, R., Gardea-Torresdey, J. L.(2014) Organic-coated silver
605 nanoparticles in biological and environmental conditions: Fate, stability and toxicity. *Advances in*
606 *Colloid and Interface Science, 204,* 15-34.
607 Shin, Y., Bae, I., Arey, B.W., Exarhos, G.J. (2008) Facile stabilization of gold-silver alloy
608 nanoparticles on cellulose nanocrystal. *The Journal of Physical Chemistry C, 112,* 4844–4848.
609 Vivekanandhan, S., Christensen, L., Misra, M., Mohanty, A.K. (2012) Green Process for
610 Impregnation of Silver Nanoparticles into Microcrystalline Cellulose and Their Antimicrobial
611 Bionanocomposite Films. *Journal of Biomaterials and Nanobiotechnology, 3,* 371-376.
612 Sun, Y., Yin, Y., Mayers, B., Herricks, T., Xia, Y. (2002) Uniform Silver Nanowires Synthesis by
613 Reducing $AgNO_3$ with Ethylene Glycol in the Presence of Seeds and Poly(Vinyl Pyrrolidone),
614 *Chemistry of Materials, 14,* 4736–4745.
615 Sun, Y., Liu, Y., Zhao, G., Zhou, X., Gao, J., Zhang, Q. J. (2008) Preparation of pH-responsive
616 silver nanoparticles by RAFT polymerization, *Journal of Materials Science, 43,* 4625–4630.
617 Tankhiwale, R., Bajpai, S.K. (2009). Graft copolymerization onto cellulose-based filter paper and
618 its further development as silver nanoparticles loaded antibacterial food-packaging material,
619 *Colloids and Surfaces B: Biointerfaces, 69(2),* 164-168.
620 - Turhan, K. N., Sahbaz, F. (2001). A simple method for determining light transmittance of polymer
621 films used for packaging foods. *Polymer International,* 50, 1138-1142.
622 - Thomas, V., Namdeo, M., Mohan, Y. M., Bajpai, S. K., Bajpai, M. (2008) Review on Polymer,
623 Hydrogel and Microgel Metal Nanocomposites: A Facile Nanotechnological Approach. *Journal of*
624 *Macromolecular Science, Part A: Pure and Applied Chemistry, 45(1),* 107-119.

Wada, M., Heux, L., Sugiyama, J. (2004) Polymorphism of cellulose I family: Reinvestigation of cellulose IV", *Biomacromolecules, 5,* 1385-1391.

Yalcinkaya, E. E., Guler, C. (2010) Electrokinetic properties of acid-activated montmorillonite dispersions,, *Separation Science and Technology, 45(5),* 635-642.

Yang, G., Xie, J., Deng, Y., Bian, Y., Hong, F. (2012). Hydrothermal synthesis of bacterial cellulose/AgNPs composite: A "green" route for antibacterial application, *Carbohydrate Polymers, 87(4),* 2482-2487.

Zare E.N., Lakouraj M.M., Mohseni M. (2014) Biodegradable polypyrrole/dextrin conductive nanocomposite: Synthesis, characterization, antioxidant and antibacterial activity, *Synthetic Metals, 187,* 9-16.

Zare E.N., Lakouraj M.M., Mohseni M., Motahari A. (2015) Multilayered electromagnetic bionanocomposite based on alginic acid: Characterization and biological activities, *Carbohydrate Polymers, 130,* 372-380.

Zhou, Z., Lu, C., Wu, X., Zhang, X. (2013) Cellulose nanocrystals as a novel support for CuO nanoparticles catalysts: facile synthesis and their application to 4-nitrophenol reduction, *RSC Advances, 3,* 26066-26073.